

secondary flow depends on the curvature of the surface, i.e., radius of curvature of the bend. Information on flows in curved pipes are highly important for many engineering applications in connection with confined curved flows through bends, headers, cooling ducts, boiler tube, heat exchanger and blade passages of turbines, air craft, power plant, particle separation, blood flow through artery, vein in human body etc. Non-Newtonian fluid flow through U-bends are mainly used in gas, oil, pulp and paper, paints, tooth-paste industries. Mainly it has been used for water, oil, gas, non-Newtonian fluid transport where change of direction of flow is necessary. Lack of information, however, exists in spite of a lot of investigations have been carried out by many researchers in many aspect.

Thomson (1876) first observed the curvature effects of bends on flow. Eustice (1910) also observed the existence of secondary flow by injecting ink into water passing through a coiled pipe. Dean (1928 a, b) studied the stability of a curved pipe flow and identified the condition for the onset of secondary vortices. Ito (1959) indicated that secondary flow can cause a rapid rise in friction and lead to a much increased pressure drop. Tunstall and Harvey (1968) observed the presence of a main or primary flow recirculation at the inner wall for tight bends ($\delta < 3$). Rowe M. (1970) also have investigated the measurements and computations of flow in pipe bends. Berger *et al.* (1983) and Das (1996) have provided a comprehensive review of literature on flow through curved pipes. The intensity of secondary flow depends on the combination of Reynolds Number (Re) and the curvature ratio ($\delta =$ radius of curvature / radius of pipe = R_{cb} / R_t) and can be characterized by the dimensionless number called the Dean Number is defined as, $De = Re (R_t / R_{cb})^{1/2}$ Where, Re is the Reynolds Number, R_t denotes the radius of pipe bend and R_{cb} is the radius of curvature of the bend. Here, we have considered four different radius of curvature of bends lying in the range $0.06 \text{ m} \leq R_{cb} \leq 0.20 \text{ m}$ which has been given in Table 1. We have seen here the effect of these four radii of curvature on static pressure and velocity vector. In geometry, the radius of curvature (R_{cb}) of a curve at a point is a measure of the radius of the circular arc which is best approximation of the curve at that point. It is the inverse of the curvature. For other curved line or surfaces, the radius of curvature at a given point is the radius of a circle (mathematically) is the best fits of the curve at that point. In the case of a surface, the radius of curvature is the radius of a circle that best fits a normal section (Fig. 3). Enayet *et al.* (1982) measured in a range of Re, 500 to 4.6×10^6 , longitudinal components of mean and fluctuating velocities for the turbulent water flow in a circular 90° bend using laser Doppler velocimeter. Azzola *et al.* (1986) reported the computations method using the standard $k-\epsilon$ model and measurements of developed turbulent flow in a 180° bend. Anwer *et al.* (1989) measured mean velocities and Reynolds stresses in the horizontal and a normal plane in an 180° bend using hot wire anemometer. Bend flows have been extensively studied experimentally by Kim and Simon (1988), Cheng and Farokhi (1992), Anwer and So (1993), Sudo *et*

al. (1998) and Sudo *et al.* (2000). The Computer simulations provide an efficient approach for studying flow through curved pipe under various conditions. Practical simulations can also be performed by solving the filtered Navier-Stokes equations using a Large-Eddy Simulation (LES) or by solving the Reynolds Average Navier-Stokes (RANS) equations with an appropriate closure model for the Reynolds stress (Jayanti *et al.*, 1990; Brockmann, 1993; Bergstrom *et al.*, 1998; Wang and Shirazi, 2001; Breuer *et al.*, 2006; Berrouk and Laurence, 2008; and Zhang *et al.*, 2009, 2010, etc.). Chen *et al.* (2004) also studied the two-phase frictional pressure drop for R-410A in four small diameter U-type return bends. Mazumder (2009) investigated erosion in a 180° U-bend using Fluent 6.3. Bandyopadhyay, T.K. and Das, S. K. (2013) studies on non-Newtonian and Gas-non-Newtonian liquid flow through Elbows with the help of CFD technique. P.Dutta *et al.*(2015) also studied the effect of Reynolds Number and Curvature Ratio on Single Phase Turbulent Flow in Pipe Bends. Jiang *et al.* (2016) studies on numerical simulation of non-Newtonian core annular flow through rectangular return bend.

Table 1 Range of variables used in the experiments

Measurement Type	Range
Diameter (m)	0.0127
Radius of curvature (m)	$0.06 \leq R_{cb} \leq 0.20$
Liquid and Flow properties	
Flow behavior index	$0.6015 \leq n' \leq 0.9013$
Consistency index (Ns^n/m^2)	$0.0142 \leq K' \leq 0.7112$
Density (kg/m^3)	$1001.69 \leq \rho \leq 1003.83$
Concentration of SCMC Solution (kg/m^3)	0.2 to 0.8
Liquid Flow Rate $Q_1 \times 10^{-4}$ (m^3/s)	2 to 4.5

2. OBJECTIVE OF THE WORK

The objective of the research work is to evaluate the performance of the availability & applicability of software. CFD analysis complements the testing and experimentation. It reduces the total effort required in the experiment design and data acquisition. It offers low cost than the physical testing methods which helps to understanding the essential engineering data for design that can be expensive. Fluent 6.3 solvers are able to solve the details flow structure, flow phenomena, static pressure, shear stress, strain, kinetic energy, Dean Vortices and pressure drop inside the U-bend. The simulated data is validated with the experimental data. It can help the design of a U-bend. The idea of this research may be help many industries to solve the problems say, waste water treatment and water particle separation from slurry, erosion in bend and for mixing purpose. The flow structure (secondary flow) in U-bend is an important implication for blood flow as the blood flow in aorta occurs through curve geometries. Also, it will be helpful to design the equipment for blood testing purpose, especially for sugar patients.

3. EXPERIMENTAL PROCEDURE

The schematic diagram of the experimental setup consists of U-bend is shown in Fig.1. The dimensions of the bend and range of variables are given in Table 1. The experiment consists of a liquid storage tank (0.45 m³), test section, control and measuring systems for flow rates, pressure and other accessories.

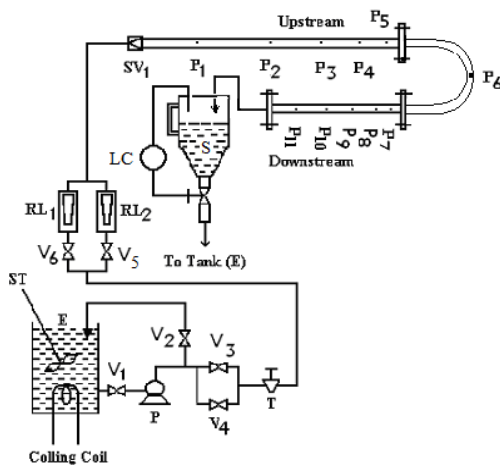


Fig. 1. Schematic diagram of the experimental set up for U-bend , E: Storage Tank, LC: Level Controller, P: Pump, P1 – P11: Pressure Tap, RL1 – RL2: Rota meters, S: Level control tank, ST: stirrer, SV1: solenoid valve, V1 – V6: Valves.

The test section consists of a horizontal upstream straight pipe of 2m length, bend portion and a horizontal downstream straight pipe of 1.4m length. The reason for having long horizontal upstream and downstream pipes before and after the bend was to achieve fully developed flow conditions to facilitate the measurement of pressure across the bend portion. The bend portion was connected to the upstream and downstream portions with the help of flanges. The piezometric ring was connected at different points of the upstream and downstream sections of the pipe and bend as pressure taps. The difference between pressures across the bends is expressed as pressure drop. The bends used were uniform internal diameter, constant curvature and roundness.

The experimental liquids were water, dilute solutions of SCMC (sodium salt of carboxy methyl cellulose, high viscous grade, Loba Chemie Pvt. Ltd., Bombay, India) acts as pseudo plastic fluids. The test liquids were prepared by dissolving the required amount of SCMC in tap water and stirring until a homogeneous solution was obtained after ageing of 12 h. Added trace amounts of formalin to prevent biological degradation. A cooling coil incorporated in the liquid storage tank controlled the liquid temperature. A level controller is used to control the level of the liquid in the tank.

Experiments were repeated a number of times to ensure reproducibility of the data. The temperature

of the water used in the experiments was maintained at $30 \pm 2^\circ\text{C}$, i.e. ambient temperature. Generally experimental temperature varying on weather condition: Summer, winter, day, night, and country to country but our experimental condition was maintained near 30°C and non-Newtonian fluid temperature maintained constant, isothermal. From the hands on experience of this pilot equipment at my laboratory, we have come to a study that this can be used at many large scale industries for application purpose.

4. EVALUATION OF FRICTIONAL PRESSURE DROP ACROSS THE U-BEND

A typical static pressure distribution curve with experimental result is shown in Fig. 2. It is an experimental plot for static pressure vs. distance. Where zero, '0' is the center position of the bend, left-hand side of the bend is negative side i.e. upstream portion and right-hand side of bend is positive side i.e. downstream portion. This plot indicates that at the fixed radius of curvature of the bend, static pressure increases with increasing non-Newtonian fluid flow rate at the different location of upstream, u-bend and downstream portion.

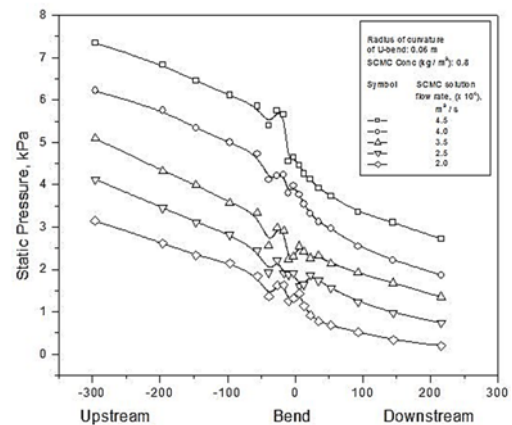


Fig. 2. Typical static pressure distribution curve.

5. LOSSES IN BENDS

5.1 Major Loss

Pressure loss through straight pipes and ducts are major losses. Pressure loss in piping components such as bends, elbows, tees, valves are minor losses. The minor loss is significant compare to the major loss. Losses through a flow system are defined as in terms of additional pressure gradient,

$$\frac{\partial p}{\partial x} = L_{loss} \rho \frac{u^2}{2} \quad (1)$$

Where, L_{loss} = loss coefficient.

The loss coefficients which are used in the CFD simulation are expressed without units and are independent of the length of the resistance of the

flow model used for U-bends. So the following loss equation is written in terms of pressure drop instead of pressure gradient:

$$\Delta P = k_{loss} \rho \frac{u^2}{2} \quad (2)$$

Where, k_{loss} = constant loss-coefficient.

The constant loss coefficient is also called as friction factor.

5.2 Minor Loss Coefficient

Pressure drop or the minor loss in components correlates with the dynamic pressure in the flow and can be expressed as,

Pressure loss:

$$P_{loss} = \Delta P = k_{loss} \rho \frac{u^2}{2} \quad (3)$$

Head loss:

$$h_{loss} = k_{loss} \left(\frac{u^2}{2g} \right) \quad (4)$$

The minor loss coefficient is expressed as,

$$k_{loss} = \frac{\Delta P}{\rho \left(\frac{u^2}{2g} \right)} \quad (5)$$

or,

$$k_{loss} = \frac{\Delta P}{\left(\frac{\rho g u^2}{2g} \right)} = \frac{\left(\frac{\Delta P}{\rho g} \right)}{\left(\frac{u^2}{2g} \right)} = \frac{h_{loss}}{\left(\frac{u^2}{2g} \right)} \quad (6)$$

Where, h_{loss} = head loss

6. CFD ANALYSIS

6.1 Mathematical Model

Dilute solutions of SCMC (Sodium salts of Carboxy Methyl Cellulose) are used here which behaves as a time independent non-Newtonian pseudo plastic fluids. The fluid follow the laminar non-Newtonian pseudo plastic power-law model. The k-ε model is used for water in bends in a turbulent region. The apparent or effective viscosity, μ_{eff} are defined from Power law model for non-Newtonian fluids as,

$$\begin{aligned} \tau_{xy} &= K' \left| \frac{\partial u}{\partial y} \right|^{n'} = \frac{K' \left| \frac{\partial u}{\partial y} \right|^{n'}}{\left| \frac{\partial u}{\partial y} \right|} = K' \left| \frac{\partial u}{\partial y} \right|^{n'-1} \left| \frac{\partial u}{\partial y} \right| \\ &= \mu_{eff} \left| \frac{\partial u}{\partial y} \right| \end{aligned} \quad (7)$$

Where,

$$\mu_{eff} = K' \left| \frac{\partial u}{\partial y} \right|^{n'-1} \quad (8)$$

Here, K' and n' are respectively the consistency index and flow behavior index. The n' is an important parameter to subdivide the fluids for Newtonian ($n' = 1$), pseudo plastic ($n' < 1$), and dilatants ($n' > 1$). The deviation of n' from unity indicates the degree of deviation from Newtonian behavior and $n' \neq 1$ indicates the shear thinning ($n' < 1$) behavior of pseudo plastic fluids.

6.2 Governing Equations

The dilute SCMC solution follows the non-Newtonian pseudo plastic Power law model and effective or apparent viscosity is introduced for calculation, as fluid viscosity depends on the shear rate. The flow behavior index for non-Newtonian pseudo plastic fluid is $n' < 1$. The effective viscosity decreases with shear rate. The effective viscosity is calculated from the equation:

$$\mu_{eff} = \left| \frac{8u}{d} \right|^{n'-1} \quad (9)$$

Where, u , d are the velocity and diameter of pipes respectively. The governing unsteady and steady state continuity and momentum Navier–Stokes equations are written as follows,

$$\nabla u = 0 \quad (10)$$

$$\rho \frac{du}{dt} + \rho u \cdot \nabla u = \mu_{eff} \nabla^2 u - \nabla P \quad (11)$$

$$\rho u \cdot \nabla u = \mu_{eff} \nabla^2 u - \nabla P \quad (12)$$

Where,

$$\nabla = i \frac{\partial}{\partial x} + j \frac{\partial}{\partial y} + k \frac{\partial}{\partial z}$$

For steady non-Newtonian SCMC solution flow, the momentum equation is,

$$u \frac{\partial}{\partial x} + v \frac{\partial u}{\partial y} = \left(\frac{1}{\rho} \right) \frac{\partial \tau_{xy}}{\partial y} \quad (13)$$

Where, u and v are the x and y velocity components and τ_{xy} is the shear stress, ρ is the density of non-Newtonian pseudo plastic fluid (SCMC solution).

6.3 Boundary Conditions

The continuity and momentum equations are solved subject to the following boundary conditions:

1. Assuming bend walls are rigid and hence no slip conditions are introduced.
2. Inlet conditions is velocity and
3. The outlet is pressure outlet.

6.4 Assumptions for Non-Newtonian Pseudo Plastic Flow Through U- Bends

The following assumptions are made while developing the theoretical model describing the flow

through the U-bend:

1. Fluid flow in the U-bend is 3-D, fully developed and steady. Fully developed flow length (entrance length) is used here to keep the cost down. Computer memory will be used low during the time of grid generation, simulation and hence lowering the convergence time.
2. Fluid is incompressible and isothermal non-Newtonian fluid.
3. The model is limited to the flow model without considering the heat transfer, as the liquid solution temperature is constant at 30°C.
4. The model follows the single phase non-Newtonian Power-law model.
5. The flow of non-Newtonian pseudo plastic fluid (SCMC solution) inside a U-bend is very complex in nature and is governed by conservation of mass and momentum in the laminar flow condition. So k-ε model is not used here.

6.5 Computational Fluid Dynamics (CFD) Procedure

The CFD simulation is used to simulate the non-Newtonian pseudo plastic liquid flow through four different types of U-bend by using the control volume based computational fluid dynamics software Fluent 6.3. The pressure based segregated implicit solver numerically solve the Navier-Stokes equation for steady and incompressible flow for getting pressure and velocity fields in U-bends. The computational flow domain was drawn and meshed by using Gambit 6.3 and following procedure is given below:

- Create a computational domain at the flow region.
- The boundary layer hexahedral meshes are created in Gambit 6.3.
- Controlling a smooth change in the mesh size by size functions.
- Specify boundary and continuum types.

Examine the mesh to ensure that the high skew ness is below 0.5.

- Export the mesh file to use in Fluent 6.3 and check the mesh.

After checking the mesh, the pressure based steady CFD solver is able to solve the 3-D Navier-Stokes equation in the following way:

- Define a 3-D, unsteady, implicit, and pressure-based solver. The memory requirement for Pressure based segregated implicit solver is lower than couple implicit solver. It provides flexibility in solution procedure.
- Activate the single-phase model.
- Define a non-Newtonian pseudo plastic Power-law model.

- Define the phase by setting non-Newtonian pseudo plastic Power law fluid, SCMC as an only single and primary phase.
- Define the operating conditions by turning on gravity and specify the operating density, non-Newtonian fluid properties.

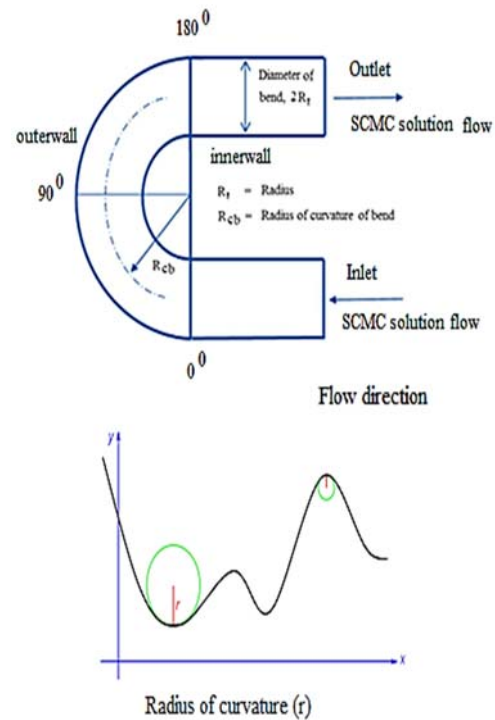


Fig. 3. Flow direction and radius of curvature inside the U-bend.

Solution control methodology – Under relaxation factors – 0.5 for pressure, 0.3 for momentum, and default values for the other parameters. Under-relaxation factor, α , is included to stabilize the iterative process for the segregated solver. Decreasing under relaxation for momentum often aids convergence.

We have used here Standard schemes – STANDARD for momentum and 1st order upwind for other variables. The first-order upwind scheme introduces severe numerical diffusion in the solution where large gradients exist. 1st order upwind scheme is an interpolation scheme used for the convection term. It is used mainly when central difference scheme cannot be able to identify the flow direction. Standard is the interpolation scheme is used for calculating the cell face pressures for pressure based implicit solver. It is a default scheme and reduced accuracy for flow exhibiting large surface-normal pressure gradients near boundaries.

Here, three algorithms are available in FLUENT for pressure-velocity coupling: Simple, Simple-C and PISO. Pressure-velocity SIMPLE coupling used here as a default scheme and solution algorithm ‘Simple’ is used for pressure-velocity coupling in steady flows. It is essentially a guess and correct procedure

for the calculation of pressure. Pressure-velocity coupling refers to the numerical algorithm which uses a combination of continuity and momentum equations to derive an equation for pressure (or pressure correction) when using the segregated implicit solver.

Finally, we have to Initialize the velocity and enable the plotting of residuals during the calculation and keep the default convergence criteria for all discrete conservation equations is used for momentum, energy (10^{-5}) and for continuity (10^{-3}).

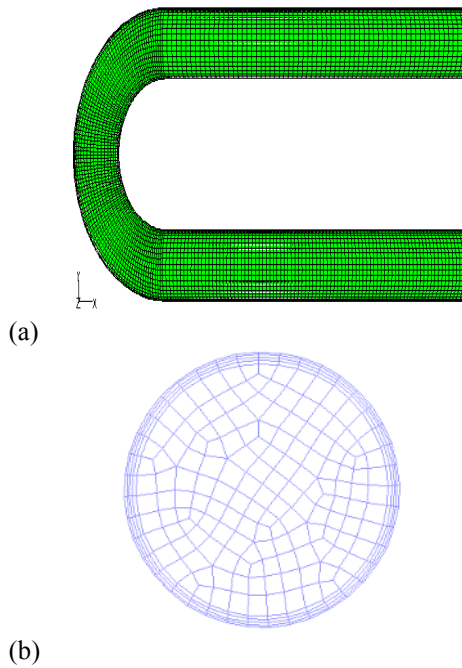


Fig. 4. The mesh geometry of (a) U-bend and (b) cross-sectional view of the U-bend, Radius of curvature of the bend: 0.06m, Radius of bend: 0.0127m, Cell elements: no. of Cells 90750, Faces 80830 and nodes 99636.

6.6 Convergence and Grid Independency

A Commercially available CFD based Ansys Fluent software is used to numerically simulate the flow through U-bends. Different U-bend geometries having different radius of curvature are created and meshed using CFD-GAMBIT modeler.

Figure 4 shows the mesh geometry for U-bend. Unstructured boundary layer hexahedral cooper meshes with nearly (9×10^4) elements are used for CFD simulation. A grid refinement study is conducted to obtain the grid independent solution. The study indicate that a large number of grid points are required to obtain accurate solution for this three dimensional simulation. To verify accuracy of the simulation, the results from CFD are first compared to experimental data. Mesh refinement does not produce important improvements of the simulated results. A computational domain ($L \geq 80D$) is used to ensure the fully developed flow results for all U-bends. Here, three different types of mesh sizes

(Coarse-45573, fine -90750 and finer-219099) have been used to study the grid independency test of liquid flow rate (2×10^4 to 4.5×10^4 m³/s) and concentration (0.2 to 0.8 kg / m³) for the U-bend to verify with the experimental results of flow and pressure fields. It can be seen that there will be no significant change found from the results between the fine and finer grids. The fine grid gives the better solution regarding to the percentage error, lower computer memory, computation time and hence simulation cost. The results are shown in the Table 2. The fine grid having size of 90,000 elements is found to be sufficient as further refinement does not give any change of velocity and pressure profiles inside the U-bends.

Table 2 Result of grid independency test

Grid size type	No. of nodes	No. of cells	CPU time, sec, RAM 4 GB	Total iteration	Time taken per iteration, sec
Coarse	52355	45573	117	211	0.55
Fine	99636	90750	263	346	0.76
Finer	234784	219099	574	657	0.87

Static Pressure (kPa)			Velocity u (m/s)		
Expt. Result	CFD result	% variation	Expt. Result	CFD result	% variation
7.10	6.98	12	3.554	3.45	10.4
7.10	7.08	2	3.554	3.53	2.4
7.10	7.07	3	3.554	3.52	3.2

The correlation coefficient (t) and variance of estimate are 0.8955 and 0.142 respectively. The value of t is 1.96 obtained from statistical table for 110 degrees of freedom, 0.05 probability levels and 96% confidence range.

7. RESULTS AND DISCUSSIONS

7.1 Hydrodynamics of SCMC Solution Fluids in U-Bends

7.1.a. Effect of Pseudo Plasticity on the Static Pressure

Figure 5 shows the effect of pseudo plasticity on static pressure. The effect is more pronounced on increasing the SCMC concentration and fluid velocity. This is due to increase of liquid viscosity at a constant flow rate for the higher concentration of SCMC solution causing more centrifugal force at the outer wall side of U-bend. Moreover increase of flow velocity of fluids (SCMC and water) at a fixed concentration causing more energy loss due to the appearance of secondary flow resulting from Dean Effect.

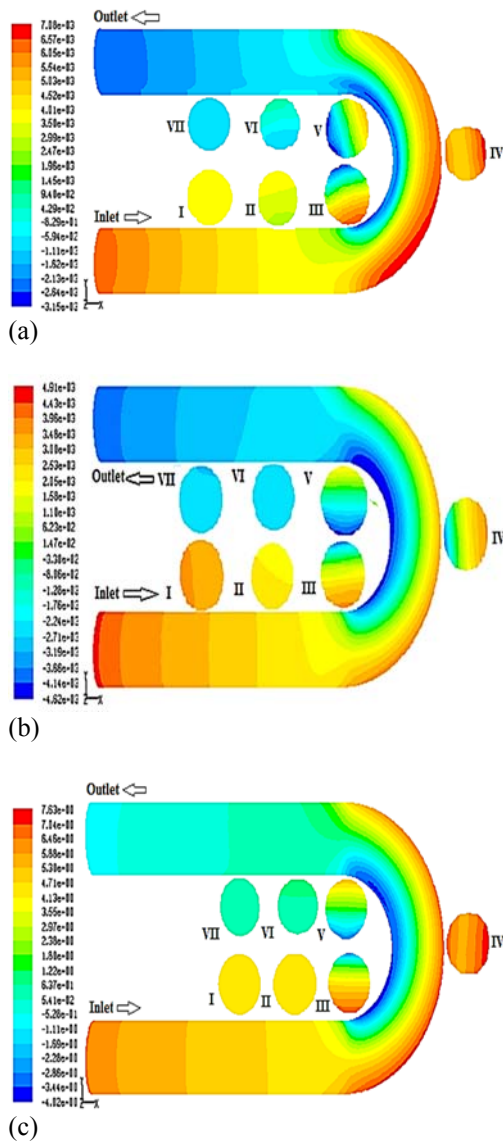


Fig. 5. Contours plot of static pressure of the U-bend for SCMC solution velocity (m/s): 3.554, radius of curvature of bend (R_{cb}) in m: 0.06, for SCMC solution Conc. (kg / m³) a) 0.8 b) 0.2 c) 0.0.

7.1.b Effect of Pseudo Plasticity on Velocity Profile Inside the U-Bend

Figure 6 shows variation of velocity, Dean Vortices at different points of U-bend with the concentration of SCMC solution. The figure illustrates that as SCMC solution entered in the bend, it tends to move towards the outer wall side due to the effect of centrifugal force and again after collision with the outer wall it returns to the inner side of the bend wall. This is due to the radius of curvature of the bend which can change the flow direction of the fluid. This effect of centrifugal force results in liquid velocity is higher at the inner side of the bend and is lower at the outer wall. So secondary flow appears and Dean Vortices play a significant role here. The effect is more intensified with increasing the concentration of SCMC solution. The velocity is more at the inner wall of the U-bend for the case of lighter density

fluid compare to the heavier one. This is due to the high energy loss for collision with the outer wall of the bend which can decelerate the speed of heavier density fluid.

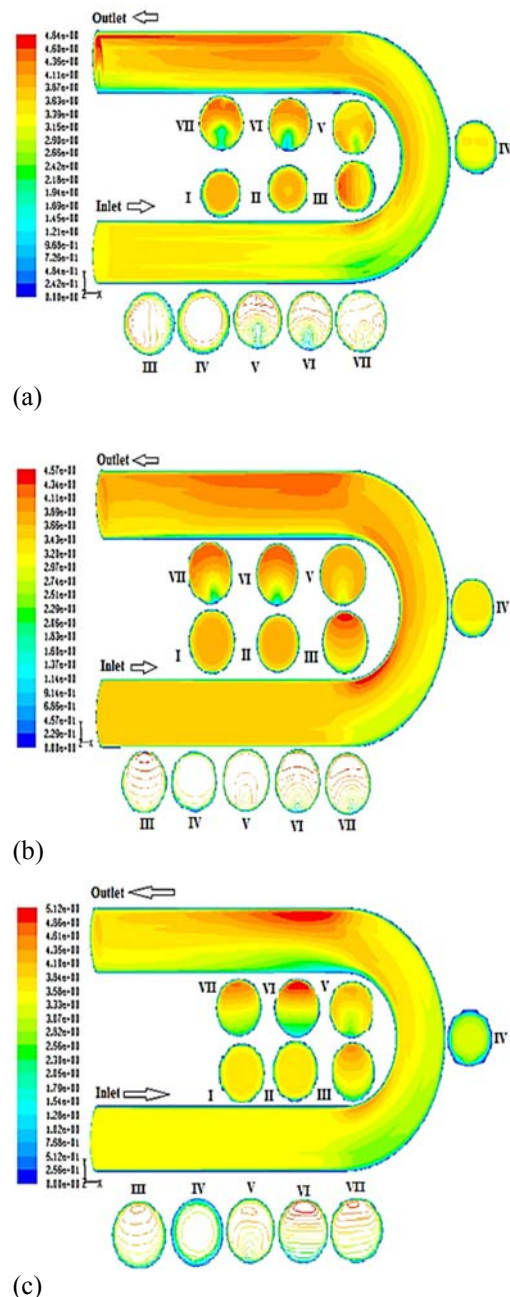


Fig. 6. Contours plot of velocity, Dean vortices of the U-bend for SCMC solution velocity (m/s): 3.554, radius of curvature of bend (R_{cb}) in m: 0.06, for SCMC solution Conc. (kg / m³) a) 0.8 b) 0.2 c) 0.0.

7.1.c Effect of Radius of Curvature of U-Bend on Pressure and Velocity Profile

Figure 7 shows a comparison of the static pressure profile for U-bends. Fig. 10 shows the similar plot for water at the different points of the bend. Fig. 8, Fig. 9, Fig. 11 and Fig. 12 show the variation of

velocity, Dean Vortices, vorticity magnitude and velocity vector with the radius of curvature of the U-bend.

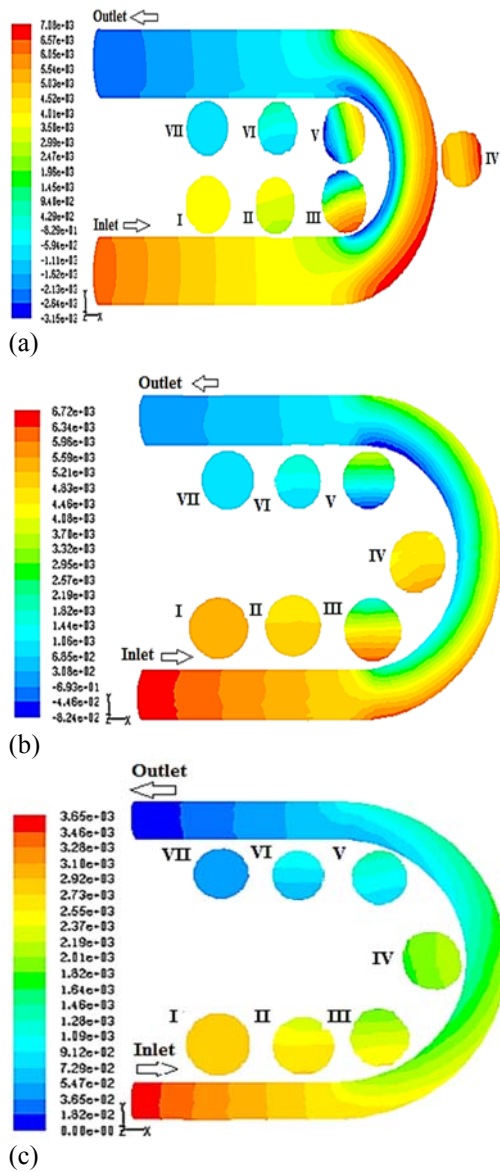


Fig. 7. Contours plot of static pressure for solution velocity (m/s): 3.554, SCMC solution Conc. (kg / m³): 0.8, radius of curvature of the U - bend (R_{cb}) in m: a) 0.06 b) 0.11 c) 0.15.

The radius of curvature of U-bend is one of the key parameters for obtaining a successful design of a bend. When the fluid entering the bend portion, the x-direction velocity profile converted to angular, radial and axial velocities of three components ω , r , and x components and distribution of velocity causing pressure distribution across the bends. The radial flow across the bends is perpendicular to the main axial flow, which produce the secondary flow and hence Dean Vortices. The radius of curvature of bend plays a role in creating and controlling complex phenomena, such as centrifugal force, secondary flow, and dean vortices.

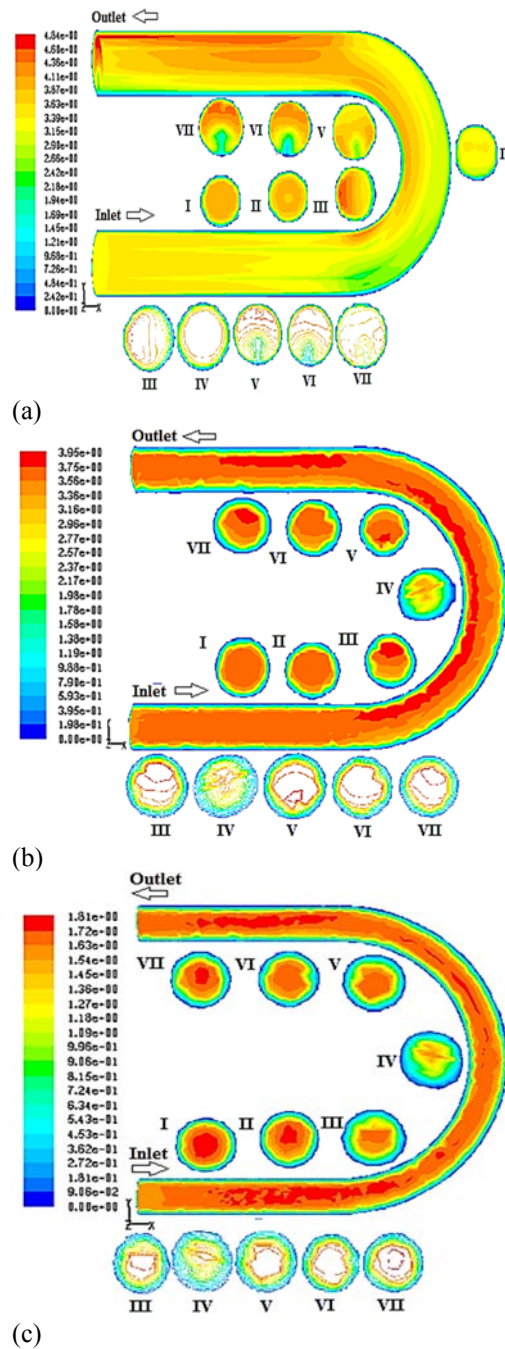


Fig. 8. Contours plot of velocity, Dean Vortices for solution velocity (m/s): 3.554, SCMC solution Conc. (kg / m³): 0.8, radius of curvature of the U - bend (R_{cb}) in m: a) 0.06 b) 0.11 c) 0.15.

A smaller radius of curvature of bend (greater curvature ratio) results in an increase in pressure drop, a faster dispersion of rope and a shorter developing flow and larger bend radius of curvature results in slower dispersion of rope and longer developing flow. This is due to small area of lower curvature bend causing flow obstruction resulting the pressure drop, sharp flow direction change causes flow separation, reversal of flow and greater turbulence results in significant pressure loss across the bend. The effect is more intensified for U-bends compare to straight pipe as the appearance of flow

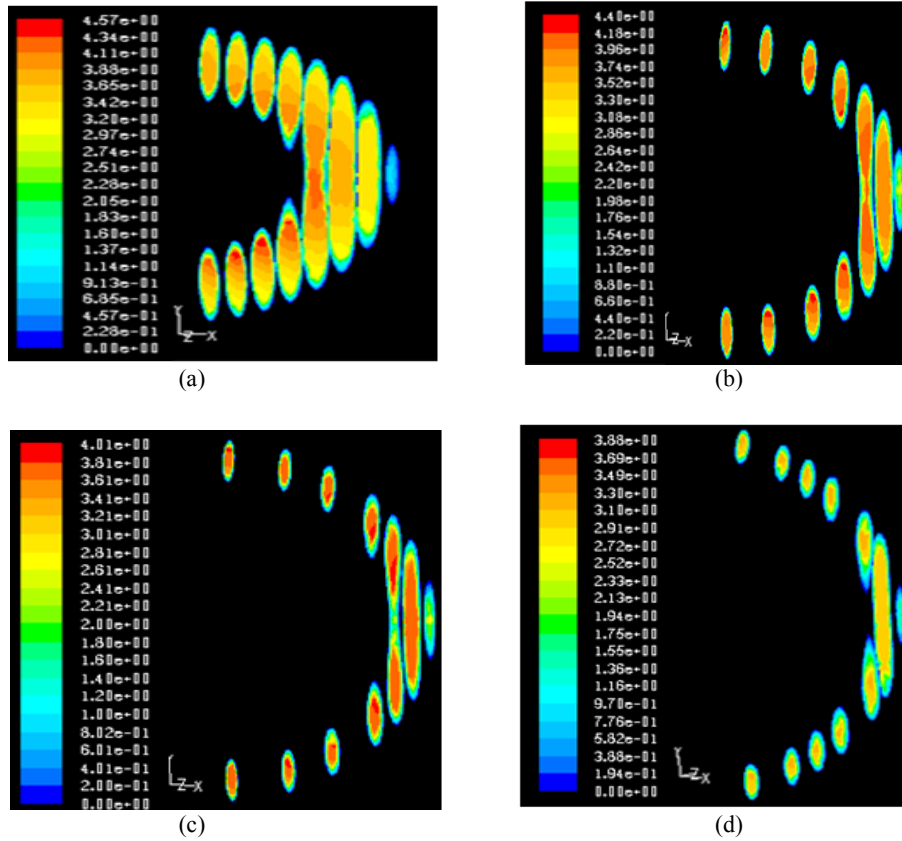


Fig. 9. Contours plot of velocity at different points of the U-bend for SCMC solution velocity (m/s): 3.554, Conc. (kg / m³): 0.8, radius of curvature of bend (R_{cb}) in m: a) 0.06 b) 0.11 c) 0.15 d) 0.20.

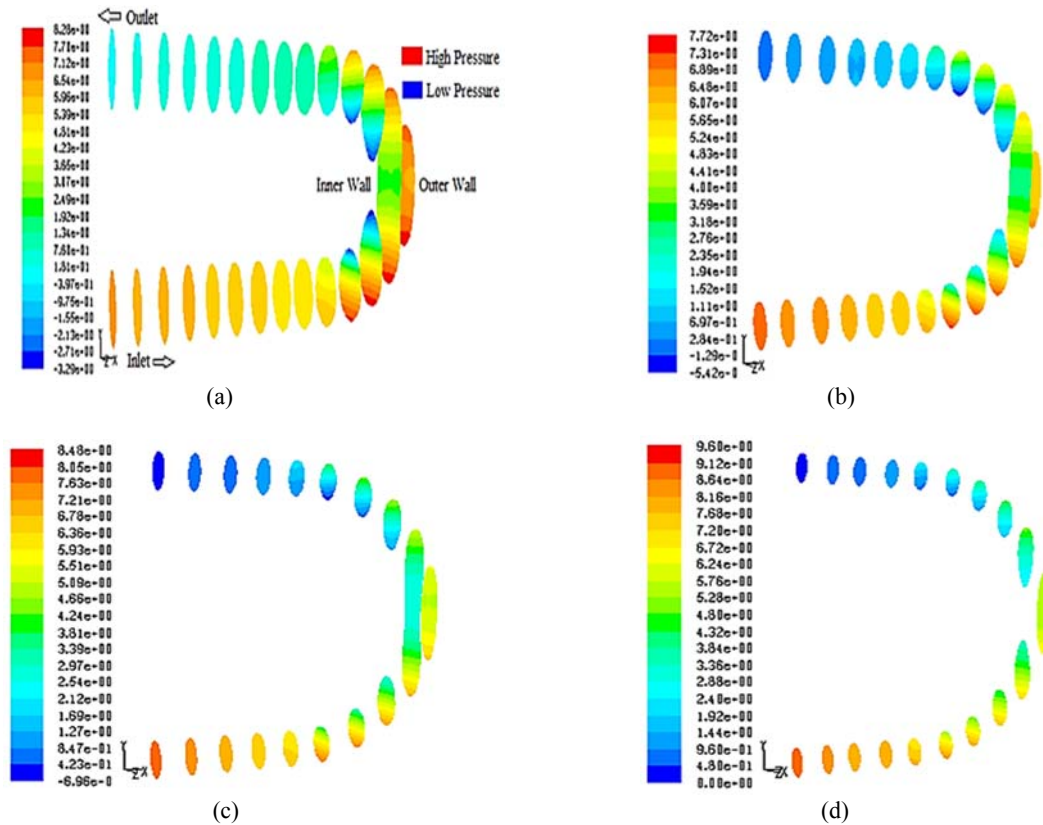


Fig. 10. Contours plot of static pressure at different points of the U-bend for water velocity (m/s): 3.554, radius of curvature of bend (R_{cb}) in m: 0.06, for (b) 0.11 (c) 0.15 (d) 0.20.

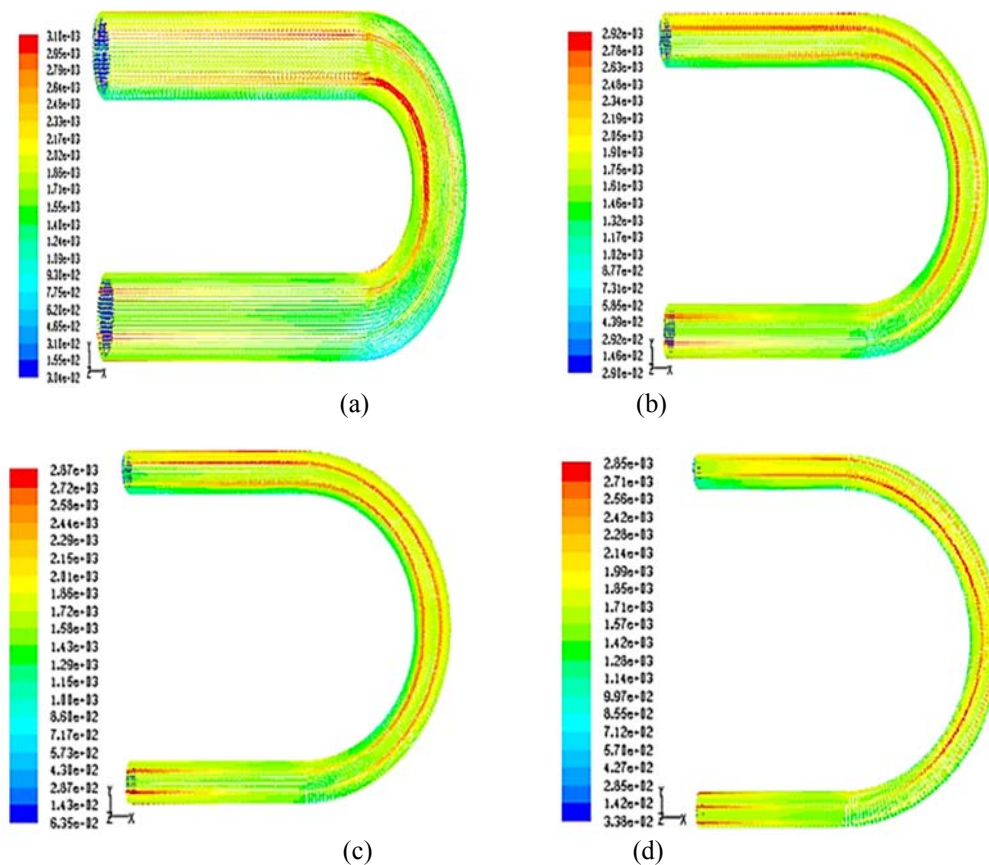


Fig. 11. Contours plot of vortices magnitude for SMC solution velocity (m/s): 3.554, Conc. (kg / m³): 0.8, radius of curvature of bend (R_{cb}) in m: a) 0.06, for b) 0.11 c) 0.15 d) 0.20.

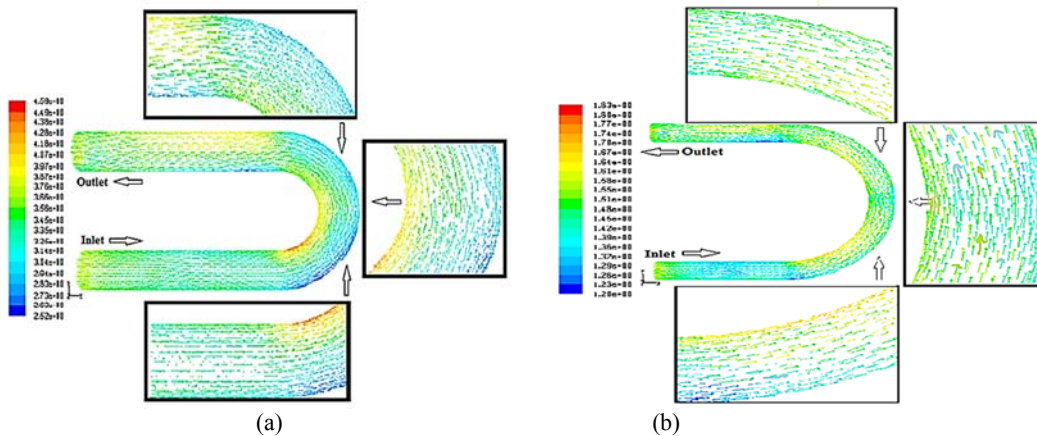


Fig. 12. Velocity vector plot for a) radius of curvature of the U - bend (R_{cb}) in m: 0.6, SMC solution Conc. (kg / m³): 0.8, SMC solution velocity (m/s): 3.554 b) radius of curvature of the U - bend (R_{cb}) in m: 0.11, SMC solution Conc.(kg / m³): 0.2, SMC solution velocity (m/s): 1.579.

obstruction phenomena: Dean effect, secondary flow (velocity, pressure distribution), pressure loss, frictional loss (skin friction), loss due to change in flow direction across the U-bend.

From those plots we observe that the intensities of static pressure, velocity, dean vortices, vorticity and velocity vector are diminished with increasing radius of curvature of U-bend. The reason is that, the increase in radius of curvature of U-bend lowers the

intensities of secondary flow phenomena and hence reduced the centrifugal forces on to the fluid inside the U-bend. The centrifugal force is (in principle) balanced by the pressure gradient in the plane of curvature. However, near the wall where the velocity is small, the pressure gradient can no longer be balanced and consequently fluid in the middle of the bend moves at the outer wall and then turns to move inward along the wall. The flow on the outer wall and separation at the inner wall make flow very complex.

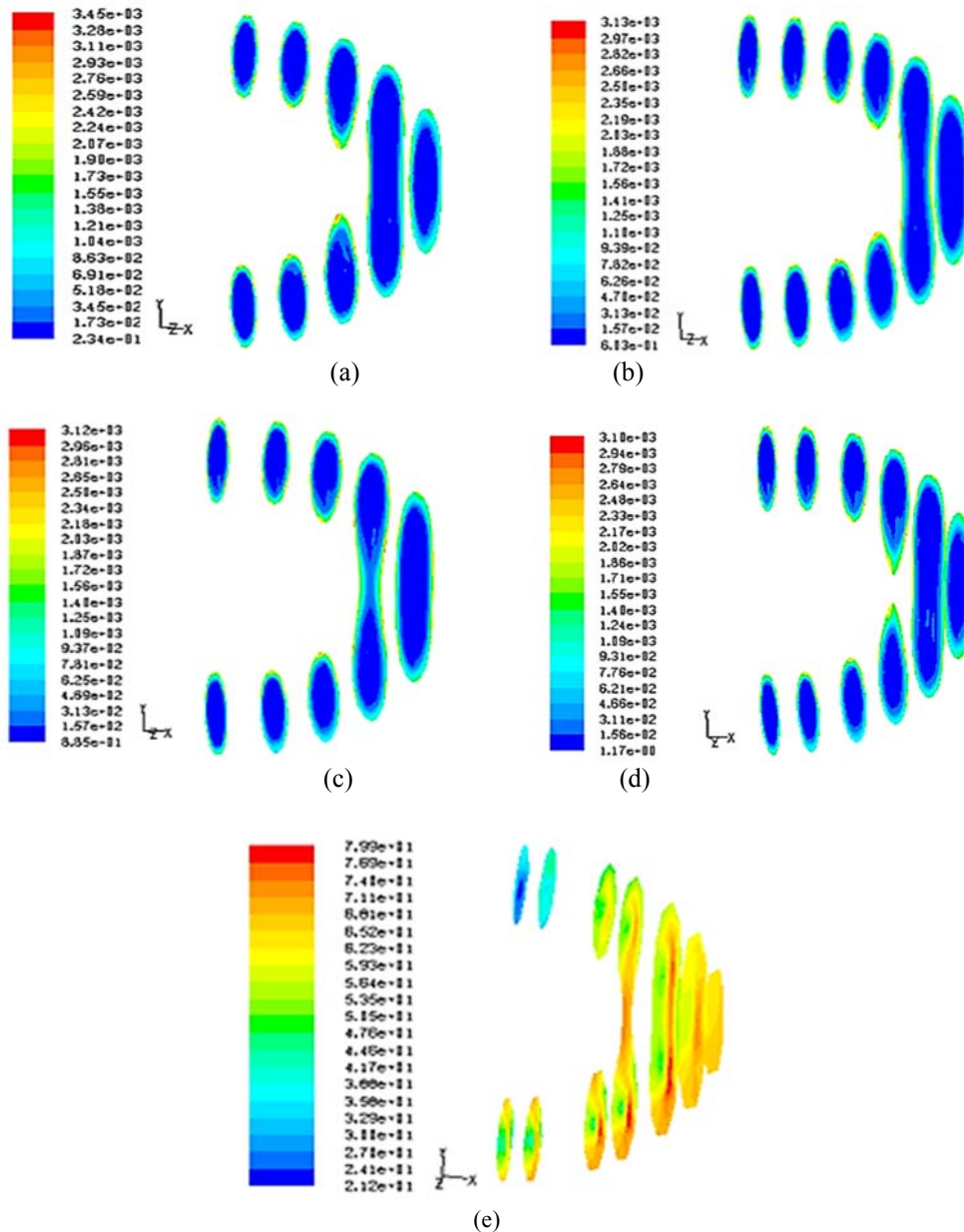


Fig. 13. Contours plot of shear strain for SCMC solution velocity (m/s): 3.554, radius of curvature of bend (R_{cb}): 0.06m, Conc. (kg / m^3): a) 0.2, for b) 0.4 c) 0.6 d) 0.8 e) 0.0.

The increase of radius of curvature of the U-bend lowers the magnitude of Dean Number,

$$De_b = \text{Re} \left(\frac{r_{bp}}{r_{cb}} \right)^{\frac{1}{2}} = \text{Re} \left(\frac{d_{bp}}{d_{cb}} \right)^{\frac{1}{2}}$$

and hence lower the curvature effect value of $\left(\frac{d_{bp}}{d_{cb}} \right)^{\frac{1}{2}}$.

The vorticity magnitude is more for more curved and less radius of curvature ratio of the bend. The velocity profile is shifted more towards the outer wall of the more curved bend and after collision with the bend wall fluid returns to the inner wall of the bend. The smaller curvature ratio and more curved

bend will increase the Dean vortices, Dean Number and hence secondary flow phenomena due to the increase of centrifugal forces compare to the less curved and large curvature ratio bend which causing more velocity and pressure distribution and more energy loss. This energy loss gives us as a form of pressure energy.

7.1.d Effect of pseudo plasticity and bend radius of curvature on shear stress and shear strain

Figure 13. (a) - (e) , shows the contour plot of shear strain for SCMC solution and water flow through the U-bends. These Figs. illustrate that the shear strains are high near to the wall of the U-bend compare to the centre position of the U-bends as velocity

variation observed near to the wall side and both depend on velocity gradient. The effects are more for high viscous fluid and both are depend on the apparent viscosity of fluids. Similarly shear stress is also high near to the wall compare to the centre position of the U-bend as shear stress is the function of shear strain.

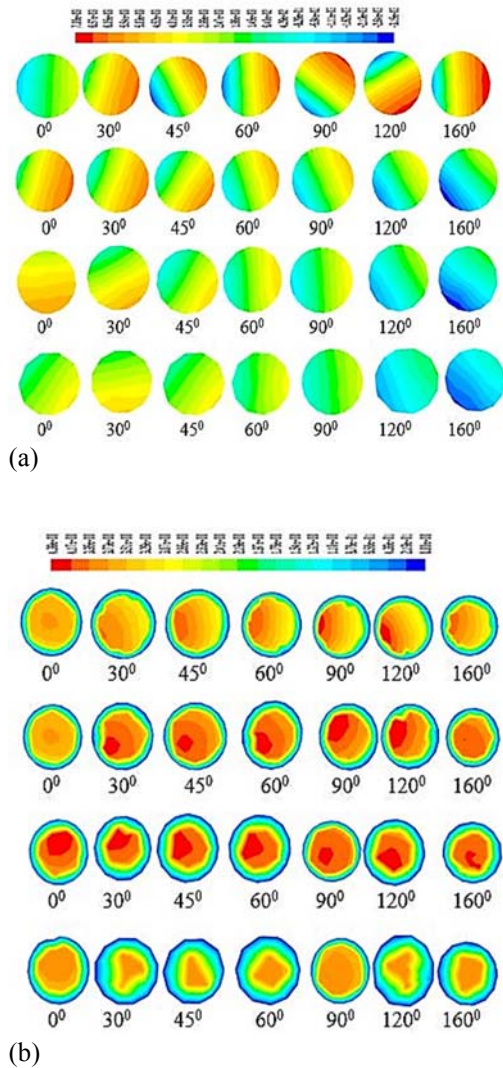


Fig. 14. a) Pressure and b) velocity field in angular coordinate for radius of curvature of bend (m): (0.06 -0.20) m, SMC solution velocity (m/s): 3.554, Conc. (kg / m³): 0.8.

7.1.e Effect of Angular Plane on Pressure, Velocity, Dean Vortices

Figure 14a, represents the contour plot of static pressure at the different angular plane of the U-bends for the different radius of curvature (0.06-0.20m). It has been observed that the static pressure decreases with the angle for fixed radius of curvature of bend and the effect is more for increasing concentration of SMC solution. But at the particular radius of curvature and angle of the bend, fully developed flow appears. It is also observed that the pressure is more intensified at the outer wall and less for inner wall

side of the bend. This is due to the effect of centrifugal force. Fig. 14b shows the contour plot of velocity profile in angular plane for the radius of curvature of bends (0.06-0.20m). The fluid initially goes to the outer wall side of the bends at the faster rate due to centrifugal force and after collision with the bend wall; the fluid comes into the inner wall side of the bend causing velocity distribution and secondary flow inside the bend. Velocity is more at the central position of the 0° angular position of the bend i.e. straight pipe but velocity starts to change from 30° – 90° and similar type velocity profile observed in between 90° – 120° angular position. Since velocity profile has minor changes between these angles and hence the flow becomes fully developed flow. The axial velocity profile becomes unsymmetrical with increasing angle due to the unbalanced centrifugal forces on the main flow and hence secondary flow to observe the vortices from the velocity profile of the bend.

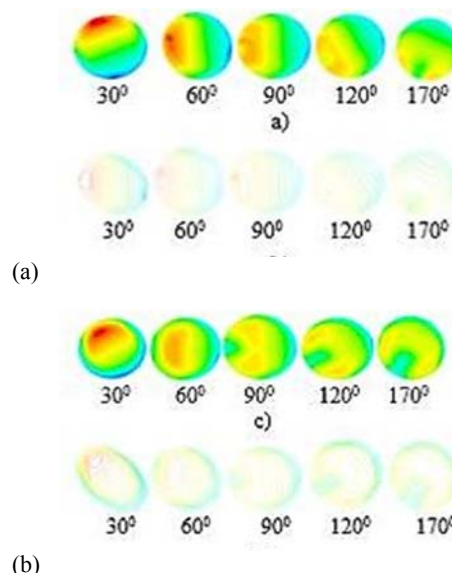


Fig. 15. Contours of dean vortices for SMC solution velocity (m/s): 3.554, radius of curvature of bend (R_{cb}): 0.06m, SMC solution Conc. (kg / m³): a) – b) 0.2 c) – d) 0.8.

Figure 15a – b, Fig. 15c – d, visualize the flow fluctuation (Dean Vortices) inside the different points of the U-bend in angular coordinates for SMC concentration (0.2-0.8 kg/m³). This is due to the inlet of the bend that the velocity profile is concentrically distributed and then the SMC solution is slightly accelerated near the inner wall. The acceleration of SMC solution in this region causes a weak secondary stream flowing from an outer to inner wall over the cross section. As the flow progresses, SMC solution experiences a centrifugal force and the static pressure in the fluid increases toward the outer wall. At the inlet of the bend the pressure gradient is more in the inner wall and gradually shifted towards the outer wall, the water near the inner wall is accelerated and decelerated near the outer wall. As the flow

progresses through the bend the strong pressure gradient along the inner wall makes the SCMC solution in the inner wall further accelerated, and the vortices are formed in the cross section by the action of the large pressure difference between the inner and outer wall. Further, flow of SCMC solution through the bend generates two counter vortices in the cross section and the SCMC solution at high velocity near the inner wall is transported toward the outer wall by the action of the secondary flow. At the bend exit a new pair of vortices appears in the outer half cross section and diminishes rapidly and the downstream, the flow returns slowly to the proper flow in a straight pipe, so it needs a longer distance for recovery. The formation of Dean Vortices more for lower density fluid compare to the high density fluid. This is due to the shear effect of high viscous fluid where the vortices are disappeared. Similar phenomena also observed by the Rowe (1970), Azzola *et al.* (1986), and Sudo *et al.* (2000).

SCMC solution decreases with increasing Reynolds number, but for water it is unchanged. The reason is that the SCMC solution behaves like a non-Newtonian pseudo plastic fluid and water as a Newtonian fluid. For a non-Newtonian fluid, the effective viscosity (μ_{eff}) is a function of shear rate ($\dot{\gamma}$) or Reynolds number (Re) but for Newtonian fluid, μ_{eff} has a constant value and is independent of the shear rate or Reynolds number.

Fig. 16b shows that the pressure drop across the U-bends increases with increasing Reynolds number. The pressure drop is high for more concentrated SCMC solution compare to the lighter fluid and water. This is due to the effect of viscosity which can increase the skin friction between the fluid layers as well as the friction between the fluid and wall. The CFD simulated data is well matched with experimental results.

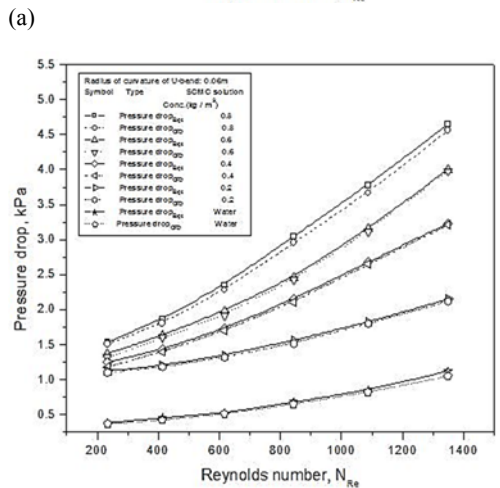
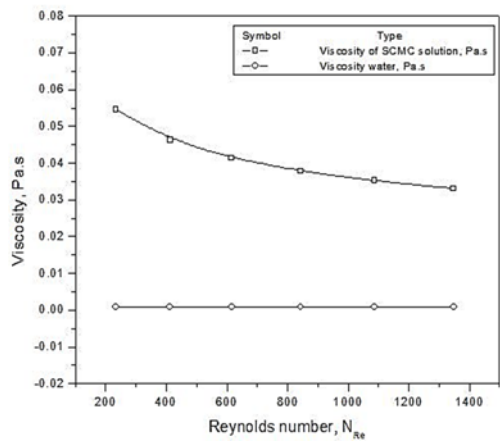


Fig. 16. a) Variation of viscosity with Reynolds number for SCMC solution and water b) Comparison plot of pressure drop vs. Reynolds number at different SCMC concentration (kg / m^3): 0.8-0.2 and water.

7.2 Validation Plot

Figure 16a shows that the effective viscosity of

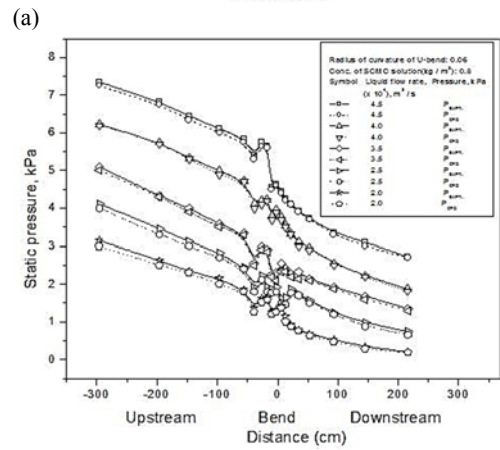
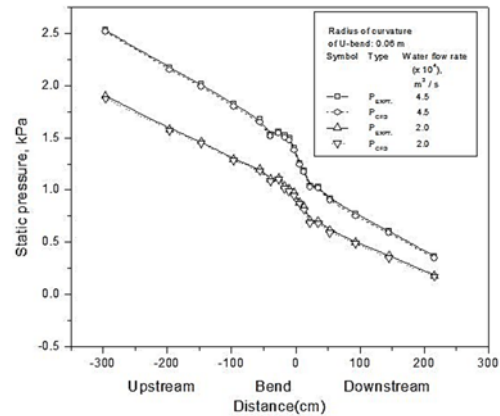


Fig. 17. Comparison plot of experimental and CFD for static pressure vs. distance of a) Newtonian fluid (water) b) non-Newtonian fluid (SCMC) solution.

Figure 17a and Fig. 17b illustrate that static pressure distribution in the upstream, downstream and U-bend portion for water and SCMC solution flow rate. The static pressure increases with increase in the flow rate of both water and SCMC solution. The effect is more with increasing SCMC solution concentration compare to the lighter fluid and water.

This is due to increase in liquid viscosity for the higher concentration of SMC solution. The experimental result matches well with CFD simulated result.

The variation of pressure drop with water and SMC solution flow rate is simulated and found to increase with decrease in radius of curvature and effect is more for SMC solution compare to water. CFD simulated results are validated with experimental results for both the cases [Fig. 18a and Fig. 18b]. The reason is that as the magnitude of the secondary flow, centrifugal forces acting on the liquids are reduced with increasing radius of curvature and hence the single-phase pressure drop decreases. The increase of radius of curvature means low curve, low Dean no. value and hence more closer to behave with straight pipe which can reduce the centrifugal and secondary forces on the fluid inside the bends and hence reduced the kinetic energy loss.

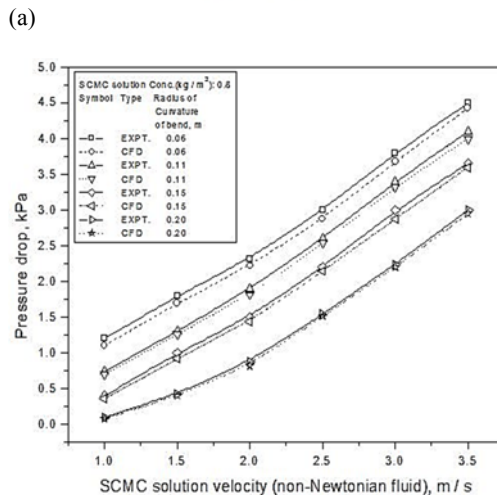
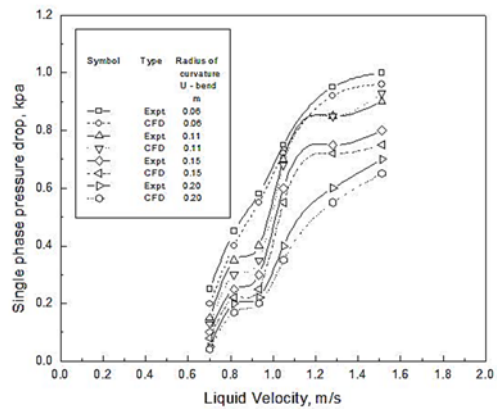


Fig. 18. Comparison plot of experimental and CFD for static pressure vs. liquid velocity of a) Newtonian fluid (water) b) non-Newtonian fluid (SCMC) solution.

Figure 19a and Fig. 19b depict the variation of velocity profile with the radial position inside the straight pipe and U-bend. The velocity profile for water flow through straight pipe is parabolic as it is Newtonian fluid, but for SMC solution, it will be flatter due to the effect of pseudo plasticity. For U-

bend, reverse effects occurs and two peaks are observed. The effect of increasing SMC solution concentration i.e. pseudo plasticity is narrowing the velocity profile at the centre position of the bend but for water it will be flatter i.e. variation is low as fluid is Newtonian.

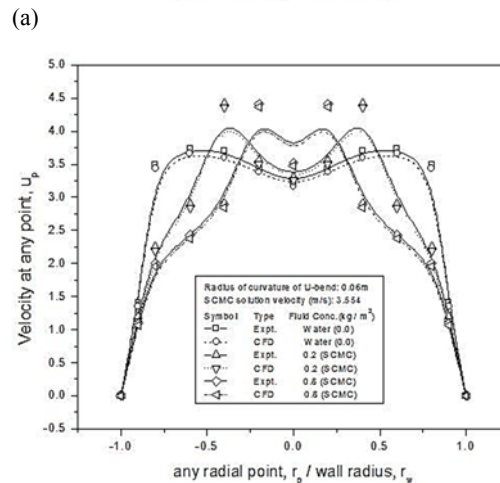
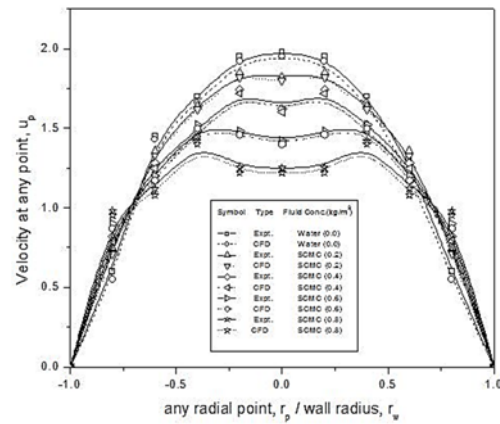


Fig. 19. Plot of velocity distribution in a) straight pipe for velocity 1.5 m/s, flow of non-Newtonian fluid (SCMC) solution and Newtonian fluid (water) b) U-bend for velocity 3.554 m/s, flow of non-Newtonian fluid (SCMC) solution and Newtonian fluid (water).

The reason is that the SMC solution shifts more to the wall side compare to water as generation of intensified centrifugal force from more angular momentum compare to less dense water. CFD simulated result matches well with the experimental data.

Figure 20a and Fig. 20b show the variation of velocity profiles at the radial and axial position of the U-bend. The velocity profile for non-Newtonian pseudo plastic fluid flow is shifted more towards the inner wall at the radial position and axial position of the U-bend compare to the Newtonian fluid. This is due to the combined effect of radius of curvature of the U-bend, pseudo plasticity, centrifugal force and secondary flow phenomena. CFD simulated data fitted well with the experimental data.

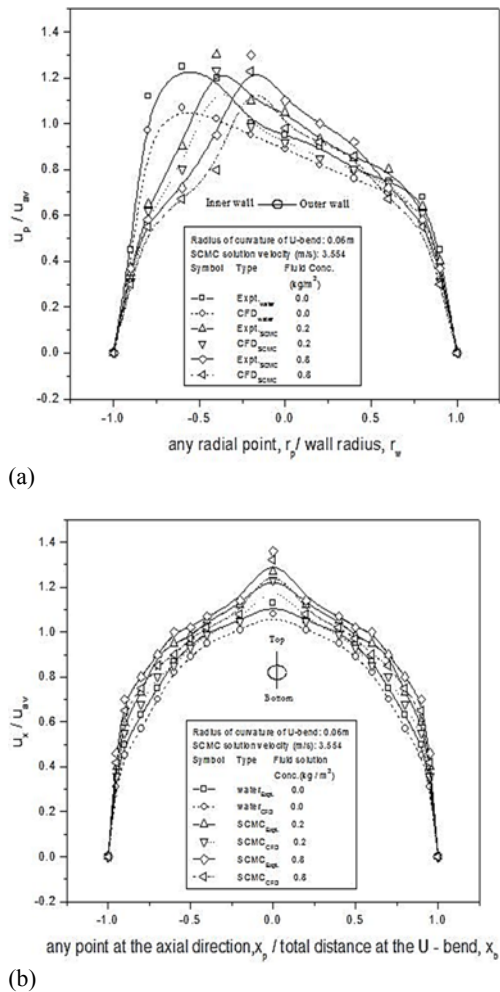


Fig. 20. Comparison plot of experimental and CFD for velocity distribution in a U-bend, radius of curvature of 0.06 m, fluid velocity 3.554 m/s, fluid concentration (kg/m³): 0.0, 0.2 and 0.8 a) radial direction (perpendicular to axial velocity) b) axial direction.

Figure 21a depicts the variation of velocity profile with radius of curvature of the bend. It has been seen that with decreasing the radius of curvature, the variation of velocity profile is more for SCMC solution compare to the flatter velocity profiles for the case of higher radius of curvature and straight pipe, but variation is less for water. This has been happened as centrifugal force is less predominant for higher curvature ratio of bend.

Figure 21b represents that the loss coefficient decreases with increasing Reynolds number, but the loss coefficient will be more for lower radius of curvature of bend compare to the higher curvature ratio of bend and straight pipe. This is due to the lowering of curvature effect, centrifugal force, and hence lowering of secondary flow, dean vortices pressure and energy loss. CFD simulated result also matches well with experimental data.

Figure 22a and Fig. 22b indicate the variation of velocity profiles in angular coordinate for water and SCMC solution flow through a fixed radius of curvature U-bends. The velocity profile for water at

0° angle is parabolic but for other angle it gives two peaks. The velocity profile goes to flatter with increasing angle due to the decrease of centrifugal force. But for SCMC solution profiles changes with peaks at 0° angle and variation of velocity is observed more due to pseudo plastic effect imposed on centrifugal force compare to water as fluid.

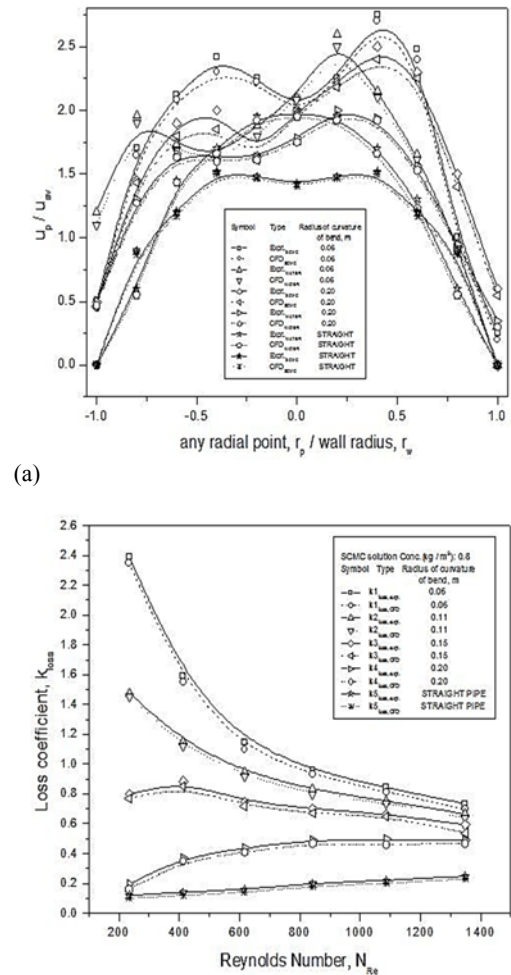


Fig. 21. Plot of velocity distribution in a) U-bend, radius of curvature of 0.06-0.20m and straight pipe for fluid velocity 3.554 m/s, fluid concentration (kg/m³): 0.8 b) loss coefficients vs. Reynolds number.

Figure 23a and Fig. 23b depict the variation of friction factor with Reynolds number for straight pipe and Dean Number for U-bend for Newtonian and non-Newtonian pseudo plastic SCMC solution fluid. The friction factor is a function of the Reynolds number (Re), Dean number (De) and SCMC solution concentration of the fluid. The friction factor decreases with increasing concentration of the SCMC solution. The reason is that the increasing non-Newtonian pseudo plastic fluid behavior of SCMC solution with increasing concentration can lower the drag by lowering the value of wall shear rate, shear stress and effective viscosity with both the numbers (Re and De). Hence friction factor decreases for non-Newtonian pseudo plastic SCMC

solution compare to water as a Newtonian fluid where viscosity of water remains unchanged. The Fig. 23a and 23b also show that the variation of friction factor is less for straight pipe than U-bend. This is due to the appearance of secondary flow, which is generated from centrifugal force in the U-bend. The CFD simulated results are validated with the experimental results.

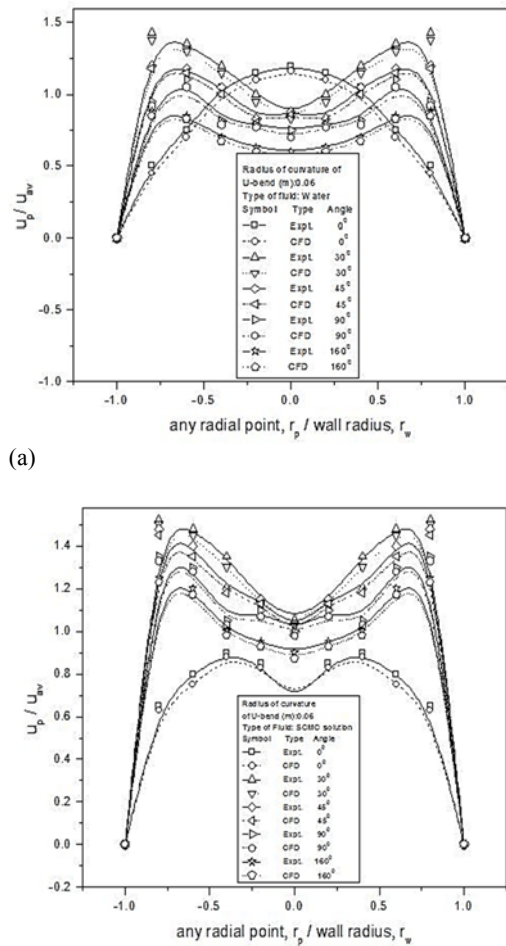


Fig. 22. Plot of angular velocity distribution in a U-bend, radius of curvature 0.06m and straight pipe for fluid velocity 3.554 m/s, a) water concentration (kg/m^3): 0.0 b) SCMC solution concentration (kg/m^3): 0.8.

8. CONCLUSIONS

The following conclusions can be drawn for this study:

1. Experimental investigations for SCMC solution and water flow through four different types of U-bends in the horizontal plane are reported. The Computational fluid dynamic simulation using Fluent 6.3 is studied to investigate the inside flow phenomena of the U-bend.
2. The pressure drop across the bends measured

for SCMC solution flow in laminar flow condition. The CFD simulations are carried out using non-Newtonian pseudo plastic Power-law model. The simulated results predicted the flow structure, pressure drop, static pressure, shear stress, shear strain, Dean Vortex phenomena and pressure profile in angular coordinates. We have also analyze the loss coefficient, friction factor for SCMC solution and water flow through straight and U-bends. The simulated pressure drop across the bends matches with the experimental data.

3. The flow fluctuation, Dean Vortices, secondary flow are visualized.
4. The effects of radius of curvature, pseudo plasticity (non-Newtonian fluid behavior) on velocity, static pressure and pressure drop are also studied here.

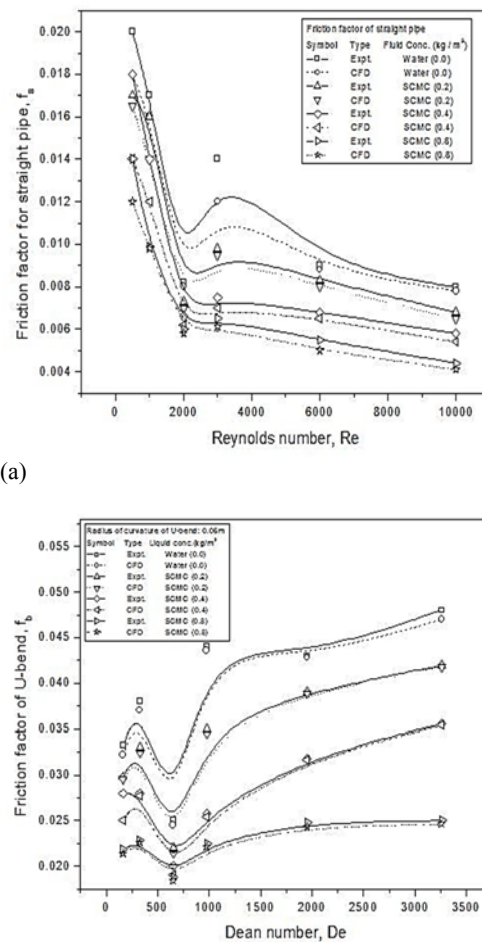


Fig. 23. Plot of a) friction factor vs. Reynolds number for straight pipe and b) friction factor vs. Dean Number for U-bend, radius of curvature 0.06m.

ACKNOWLEDGEMENT

The authors gratefully acknowledge the financial support of the MHRD India for this project.

REFERENCES

- ANSYS, (2007). *Inc., ANSYS FLUENT 6.3, Theory Guide*.
- Anwer, M., R. M. C. So and Y.G. Lai (1989). Perturbation by and recovery from bend curvature of a fully developed turbulent pipe flow, *Phys Fluids, A1*, 1387-1397.
- Anwer, M. and R. M. C. So (1993). Swirling turbulent flow through a curved pipe Part I; effect of swirl and bend curvature, *Expt. Fluids 14*, 85-96.
- Azzola, J., J. A. C. Humphery, H. Iacovides and B. E. Launder (1986). Developing turbulent flow in a U-bend of circular cross-section : measurement and computation, *Trans. J. Fluid Engg., ASME, 108*, 214-221.
- Bandyopadhyay, T. K. and S. K. Das (2013). Non-Newtonian and Gas-non-Newtonian liquid flow through Elbows – CFD analysis, *Journal of Applied Fluid Mechanics, 6*(1), 131-141.
- Berger, S. A., A. Talbot and L. S. Yao (1983). Flow in curved pipes, *Ann. Rev. Fluid Mech. 15*, 461-512.
- Bergstrom, D. J. (1998). Application of power loss to low Reynolds number for the wake of a normal flat plate, *Journal of fluid Mechanics 370*.
- Berrouk, A. B. and D. Laurence (2008). Stochastic modeling of aerosol deposition for LES of 90° bend turbulent flow, *Int. J. Heat and Fluid Flow 29*, 1010-1028.
- Breuer, M., H. T. Baytekin and E. A. Matida (2006). Prediction of aerosol deposition in 90° bends using LES and an efficient Lagrangian tracking method, *J. Aerosol Sci. 37*, 1407-1428.
- Brockmann, J. E. (1993). *Sampling and transport of aerosol, in aerosol measurement: principles, techniques, and applications*, in Baron P. A. and Willeke K., editors, New York, Van Nostrand Reinhold.
- Chen, Y. I., C. C. Wang and S. Y. Lin (2004). Measurement and correlations of frictional single-phase and two-phase pressure drops of R-410A flow in small U-type return bends, *Int. J. Heat Mass Transfer 47*, 2241–2249.
- Cheng, G. C. and S. Farokhi (1992). On turbulent flows dominated by curvature effects, *J. Fluids Engg. 114*, 52-57.
- Das, S. K. (1996). *Water flow through helical coils in turbulent condition, in Multiphase Reactor and Polymerization System Hydrodynamics*, N. P. Cheremisinoff Editor, Gulf Publication USA, Ch. 17, 379-403.
- Dean, W. R. (1928b). The Stream-line motion in curved pipes, *Philos. Mag. 30*, 673-693.
- Dean, W. R. (1928a). Fluid motion in a curved channel, *Proc. R. Soc. London 121*, 402-420.
- Enayet, M. M., M. M. Gibson, A. M. K. P. Taylor and M. Yianneskis (1982). Laser-doppler measurements of laminar and turbulent flow in a pipe bend, *Int. J. Heat Fluid Flow 3*, 213-219.
- Eustice, J. (1910). Flow of water in curved pipes, *Proc. R. Soc. London 84*, 107-118.
- Ito, H. (1959). Friction factors for turbulent flow in curved pipes, *ASME J. of Basic Engg. 81*, 123-134.
- Jayanti, S., G. F. Hewitt and J. R. Kightley (1990). Fluid flow in curved ducts, *Int. J. Num. Methods in Fluids 10*, 567-589.
- Jiang, F., Y. Long, Y. J. Wang, Z. Z. Liu and C. G. Chen (2016). Studied on numerical simulation of non-Newtonian core annular flow through rectangle return bend, *Journal of Applied Fluid Mechanics 9*(1), 431-441.
- Kim, J. and T. W. Simon (1988). Measurements of the turbulent transport of heat and momentum in convexly curved boundary layers : effects of curvature, recovery and free-stream turbulence, *J. Turbomachinery 110*, 81-87.
- Mazumder, Q. (2009). *Investigation of erosion in a 180° U-bend using Fluent*, U-BEND FLUENT Tutorial: CFDRC- Univ. of Michigan-Flint, USA 1-13.
- Dutta, P. et al.(2015). The effect of Reynolds Number and Curvature Ratio on Single Phase Turbulent Flow in Pipe Bends, *Mechanics and Mechanical Engineering 19* (1), 5–16.
- Rowe, M. (1970). Measurements and Computations of flow in pipe bends, *J. Fluid Mech. 43*, 771-783.
- Sudo, K., M. Sumida and H. Hibara (1998). Experimental investigation on turbulent flow in a circular-sectioned 90-degrees bend, *Expt. Fluids 25*, 42-49.
- Sudo, K., M. Sumida and H. Hibara (2000). Experimental investigation on turbulent flow through a circular sectioned 180° bend, *Expt. Fluids 28*, 51-57.
- Thomson, J. (1876). On the origin of windings of rivers in alluvial plains, with remarks on the flow of water round bends in pipes, *Proc. R. Soc. London 25*, 5-8.
- Wang, J. and S. Shirazi (2001). A CFD based correlation for mass transfer coefficient in elbows, *Int. J. Heat Mass Transfer 44*, 1817-1822.
- Zhang, P., Y. Gros, R. M. Roberts and A. Benard (2010). *Modeling of turbulent flow with particle deposition in curved pipes*, *Proc. 7th Int. Conf. on Multiphase flow ICMF*, Tampa, FL USA, May30-June.